

Supplementary Material

Integrating PtNi Nanoparticles on NiFe Layered Double Hydroxide Nanosheets as Bifunctional Catalyst for Hybrid Sodium-Air Batteries

Xueqing Yu,^{‡a} Yao Kang,^{‡a} Shuo Wang,^{‡a} Kwan San Hui,^b Kwun Nam Hui,^{*a} Huajun Zhao,^{ac} Jianding Li,^a Bo Li,^a Jincheng Xu,^a Liang Chen,^{*de} and Huaiyu Shao^{*a}

^aJoint Key Laboratory of the Ministry of Education, Institute of Applied Physics and Materials Engineering, University of Macau, Avenida da Universidade, Taipa, Macau SAR, China. Email: bizhui@um.edu.mo, hshao@um.edu.mo

^b Engineering, Faculty of Science, University of East Anglia, Norwich, NR4 7TJ, United Kingdom

^c Department of Materials Science and Engineering, Southern University of Science and Technology, Shenzhen, Guangdong 518055, China

^d Ningbo Institute of Materials Technology and Engineering, Chinese Academy of Sciences, Ningbo, Zhejiang 315201, China. Email: chenliang@nimte.ac.cn

^e University of Chinese Academy of Sciences, Beijing, 100049, China

[‡] These authors contributed equally.

^{*} Corresponding author.

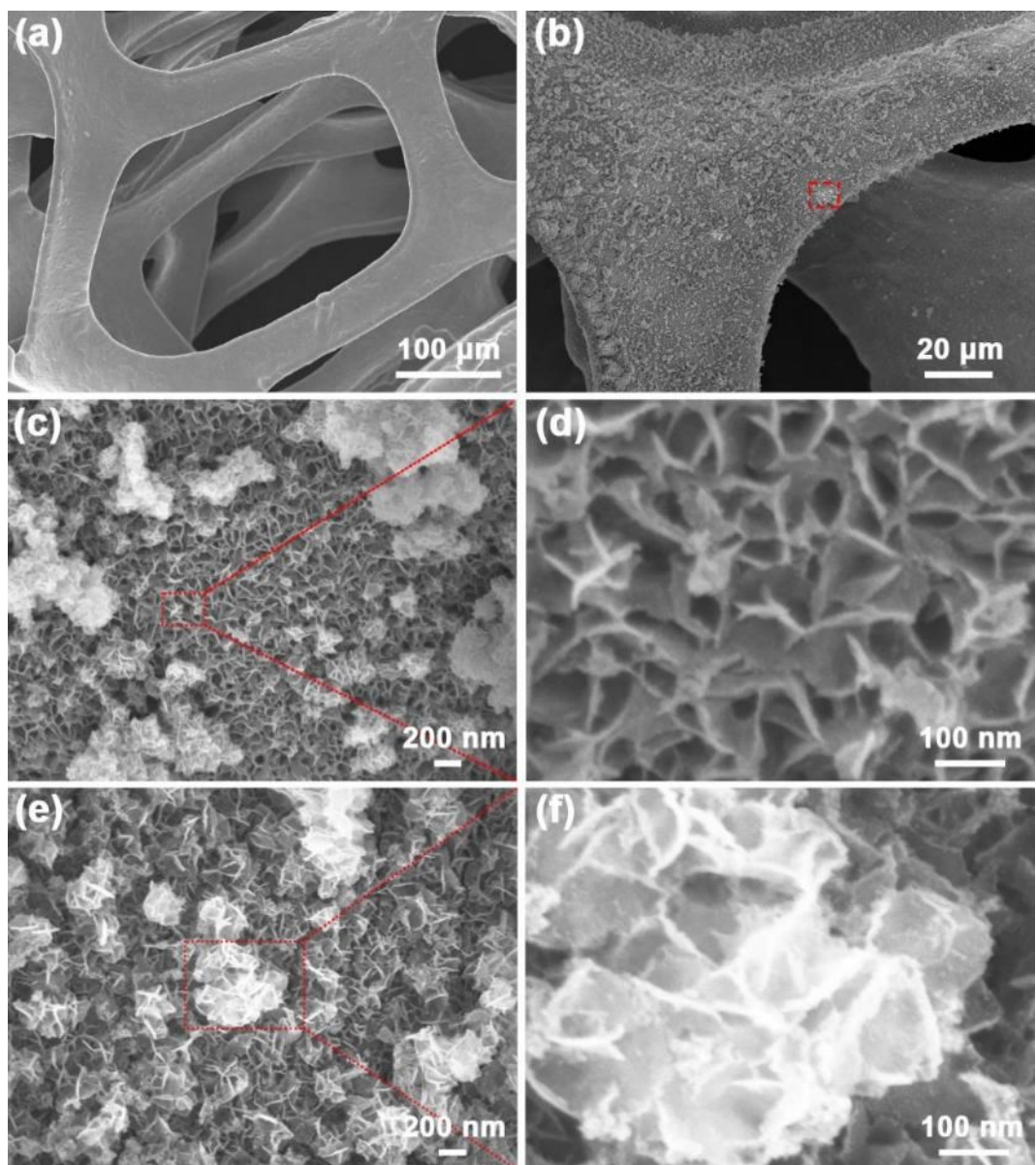


Fig. S1 SEM images of (a) pristine Ni foam, (b-d) NiFe LDHs, and (e, f) NiZnFe LDHs.

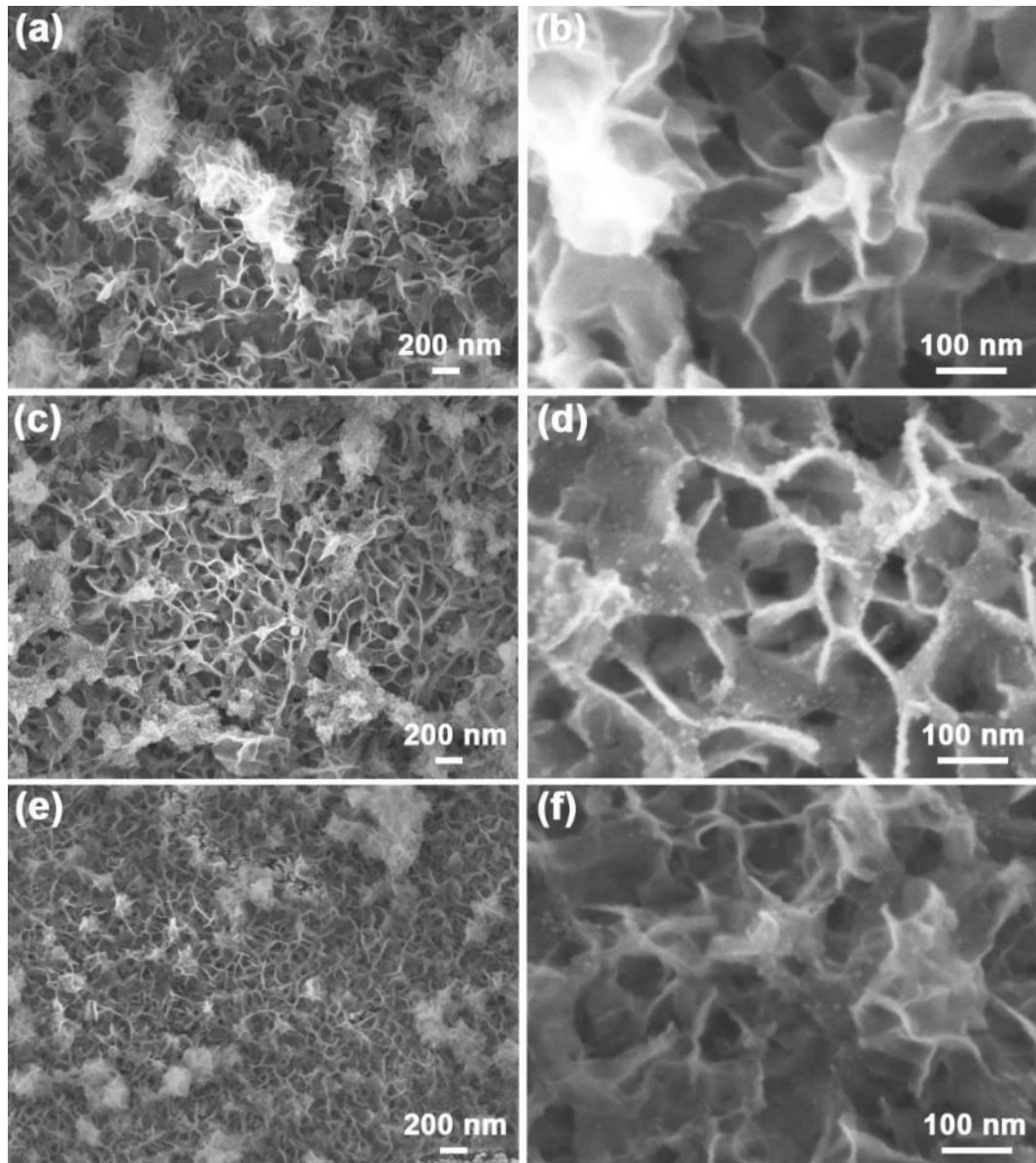


Fig. S2 SEM images of (a, b) Ni_xFe LDHs, (c, d) Pt/Ni_xFe LDHs, and (e,f) Pt₃Ni₁/Ni_xFe LDHs at different magnifications.

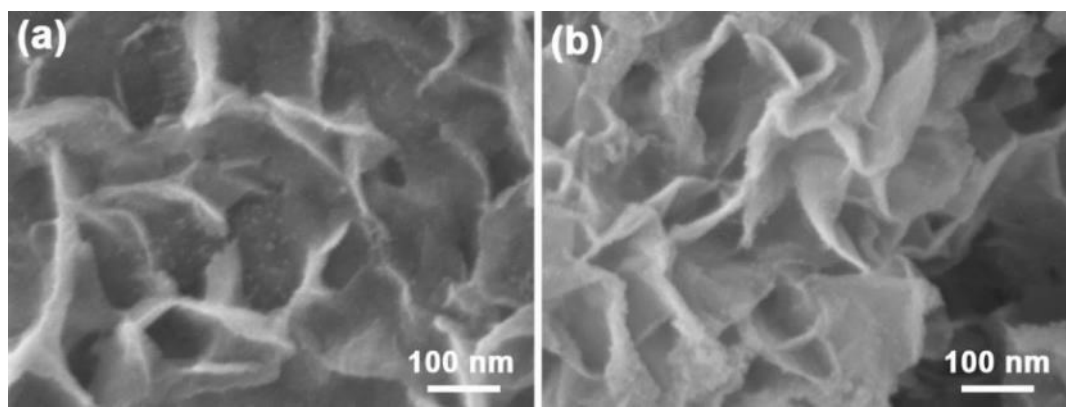


Fig. S3 SEM images of (a) $\text{Pt}_1\text{Ni}_1/\text{Ni}_x\text{Fe}$ LDHs and (b) $\text{Pt}_1\text{Ni}_3/\text{Ni}_x\text{Fe}$ LDHs.

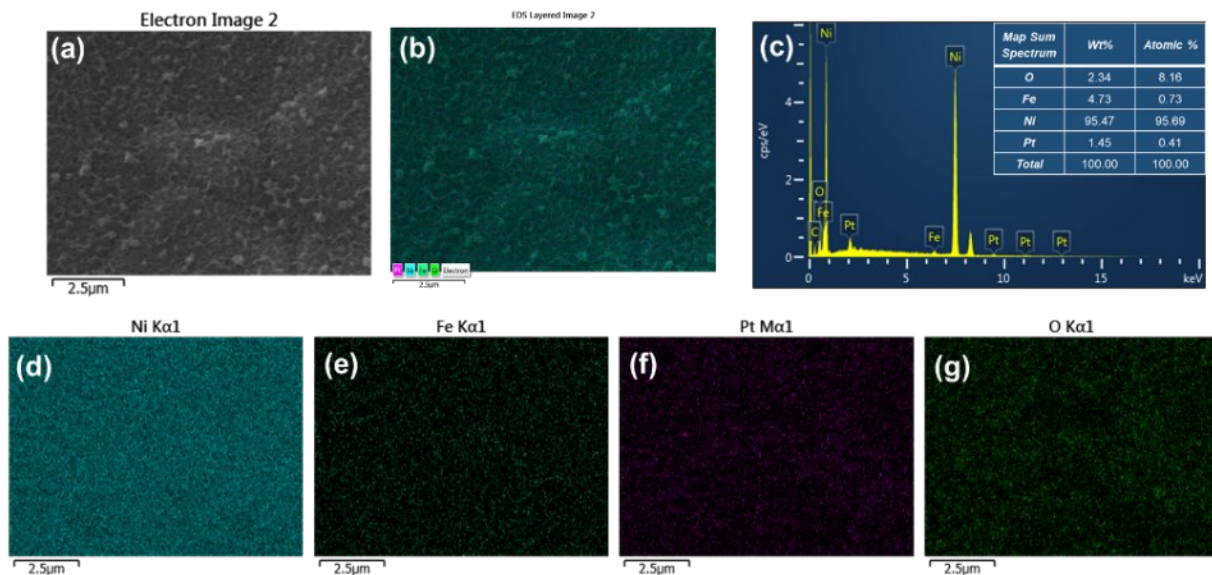


Fig. S4 (a) SEM and (b-g) corresponding EDS elemental mapping images of $\text{Pt}_3\text{Ni}_1/\text{Ni}_x\text{Fe}$ LDHs nanocomposites.

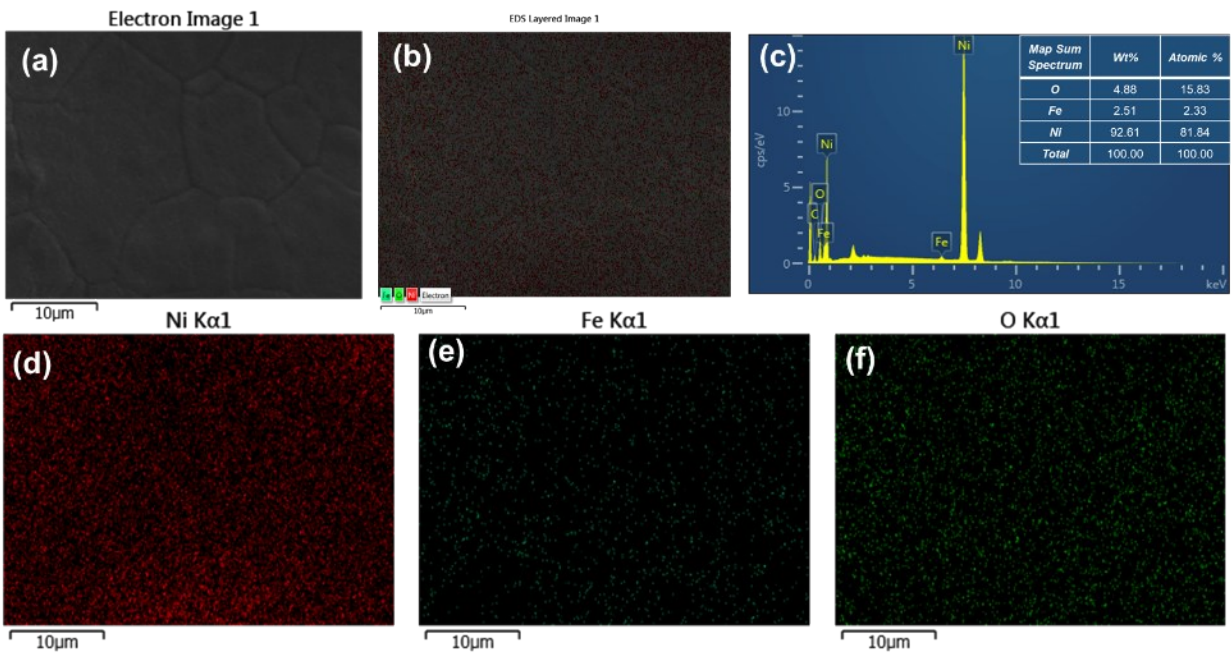


Fig. S5 (a) SEM and (b-f) corresponding EDS elemental mapping images of Ni_xFe LDHs nanocomposites.

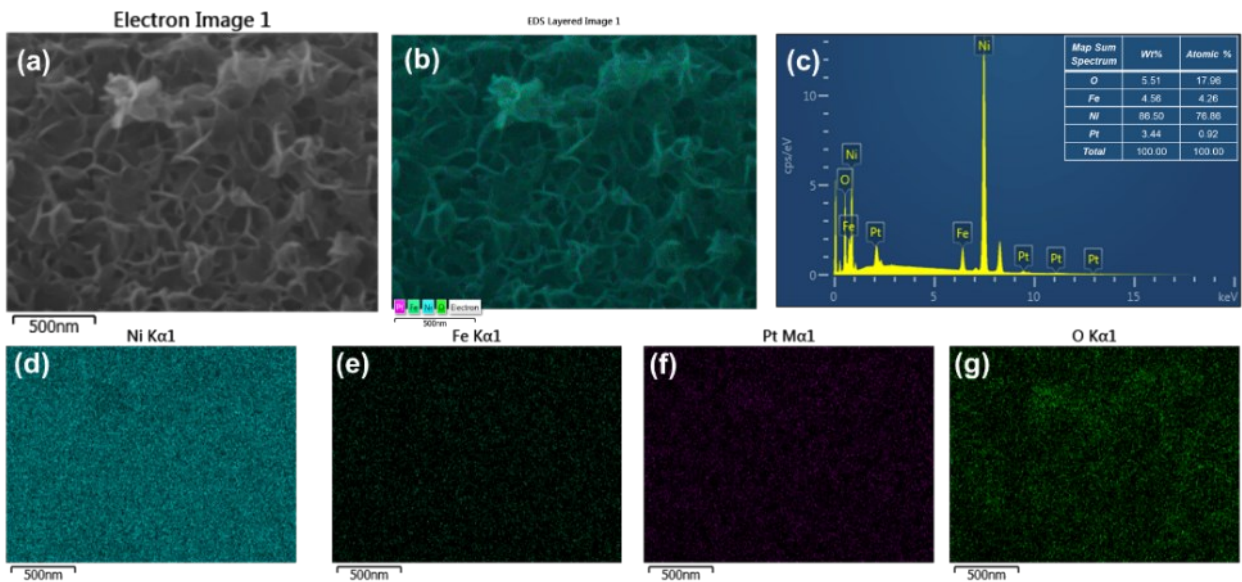


Fig. S6 (a) SEM and (b-g) corresponding EDS elemental mapping images of Pt/ Ni_xFe LDHs nanocomposites.

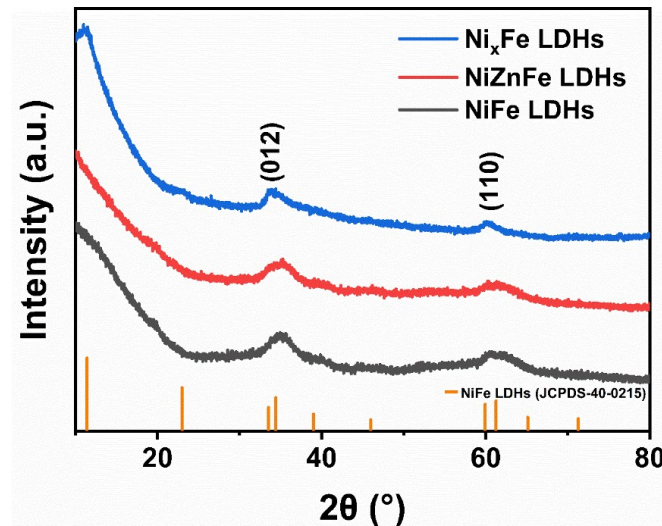


Fig. S7 The XRD patterns of NiFe LDHs, NiZnFe LDHs, and $\text{Ni}_x\text{Fe LDHs}$ nanosheets.

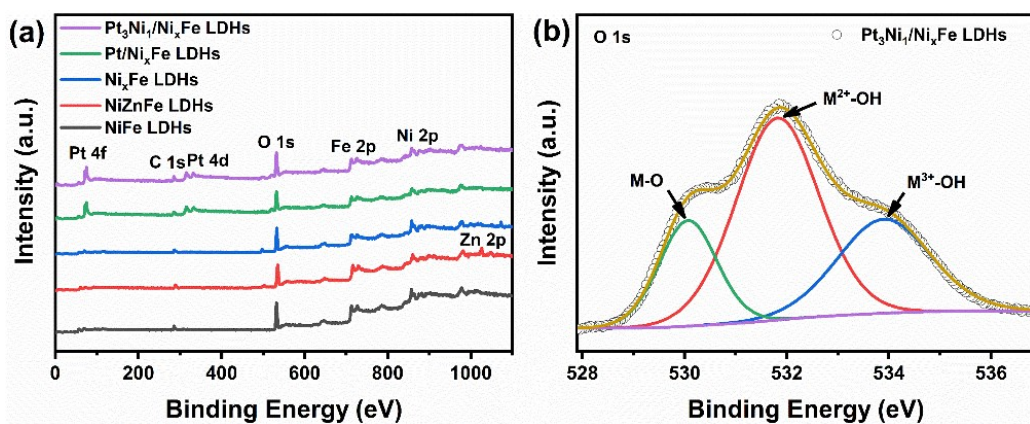


Fig. S8 (a) The overall XPS spectra of NiFe LDHs, NiZnFe LDHs, $\text{Ni}_x\text{Fe LDHs}$, $\text{Pt}/\text{Ni}_x\text{Fe LDHs}$, and $\text{Pt}_3\text{Ni}_1/\text{Ni}_x\text{Fe LDHs}$. (b) High-resolution XPS spectra of O 1s core levels in $\text{Pt}_3\text{Ni}_1/\text{Ni}_x\text{Fe LDHs}$.

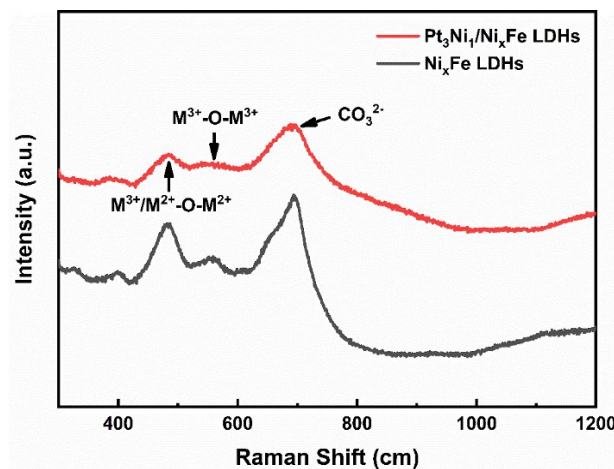


Fig. S9 Raman spectra of NiFe LDHs and $\text{Pt}_3\text{Ni}_1/\text{Ni}_x\text{Fe LDHs}$ obtained at 633 nm.

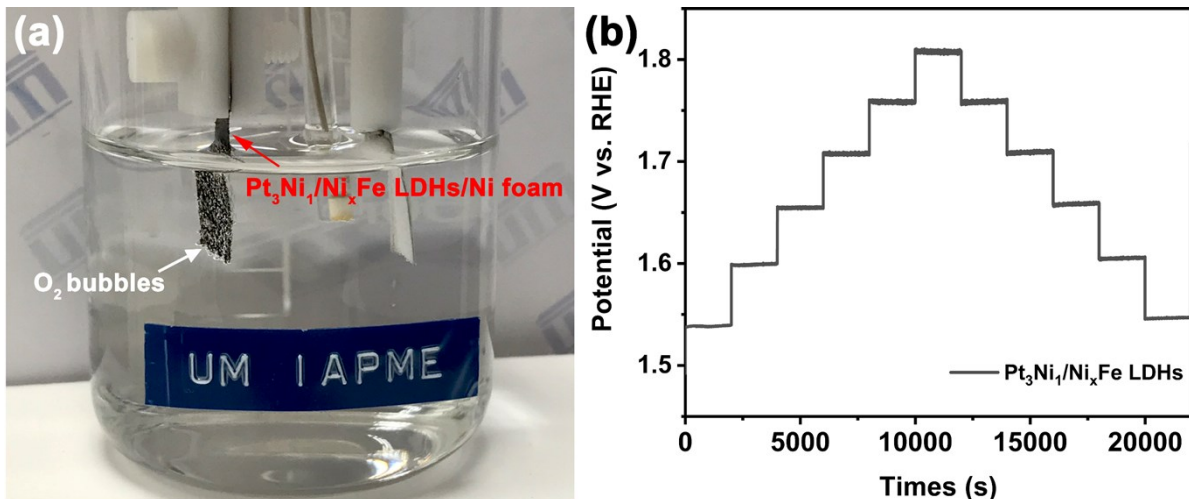


Fig. S10 (a) Digital photo of $\text{Pt}_3\text{Ni}_1/\text{Ni}_x\text{Fe}$ LDHs for catalyzing OER process. (b) Multi-current process obtained with the $\text{Pt}_3\text{Ni}_1/\text{Ni}_x\text{Fe}$ LDHs electrode in 1 M KOH. The current density started at 50 mA cm^{-2} increased to 250 mA cm^{-2} , then down to 50 mA cm^{-2} , with a gradient of 50 mA cm^{-2} every 500 s.

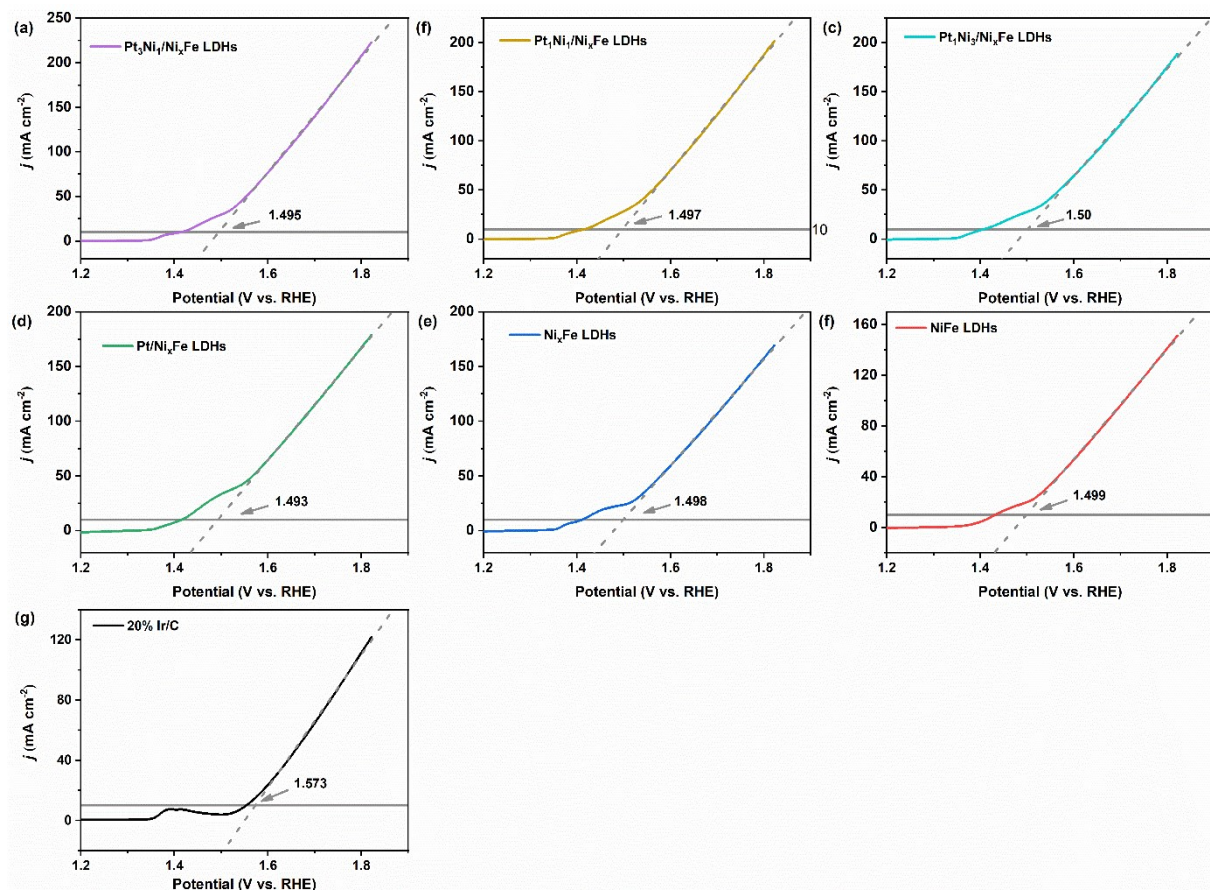


Fig. S11 OER LSV curves of (a) $\text{Pt}_3\text{Ni}_1/\text{Ni}_x\text{Fe}$ LDHs, (b) $\text{Pt}_1\text{Ni}_1/\text{Ni}_x\text{Fe}$ LDHs, (c) $\text{Pt}_1\text{Ni}_3/\text{Ni}_x\text{Fe}$ LDHs, (d) $\text{Pt}/\text{Ni}_x\text{Fe}$ LDHs, (e) Ni_xFe LDHs, (f) NiFe LDHs and (g) commercial 20% Ir/C, and the corresponding applied voltages at 10 mA cm^{-2} were estimated by extrapolating the polarization curves, respectively.

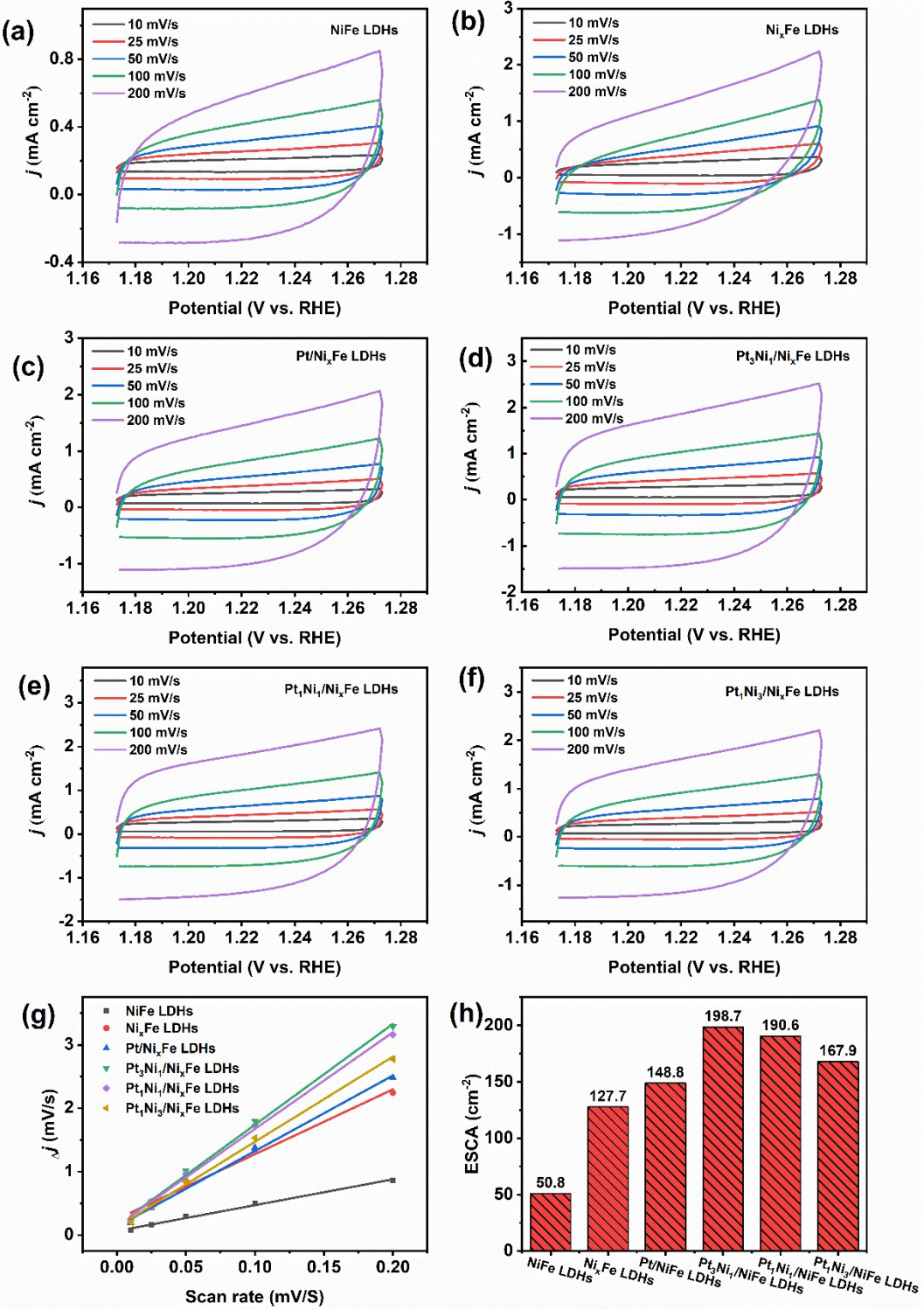


Fig. S12 Cyclic voltammograms obtained with (a) NiFe LDHs, (b) Ni_xFe LDHs, (c) Pt/ Ni_xFe LDHs, (d) $\text{Pt}_3\text{Ni}_1/\text{Ni}_x\text{Fe}$ LDHs, (e) $\text{Pt}_1\text{Ni}_1/\text{Ni}_x\text{Fe}$ LDHs, and (f) $\text{Pt}_1\text{Ni}_3/\text{Ni}_x\text{Fe}$ LDHs in the capacitance current range (1.173-1.273 V) at scan rates of 10, 25, 50, 100 and 200 mV s^{-1} , respectively. (g) The plot of the difference between double layer charging currents ($j_a - j_c$) vs. scan rate. (h) ESCA of various catalysts.

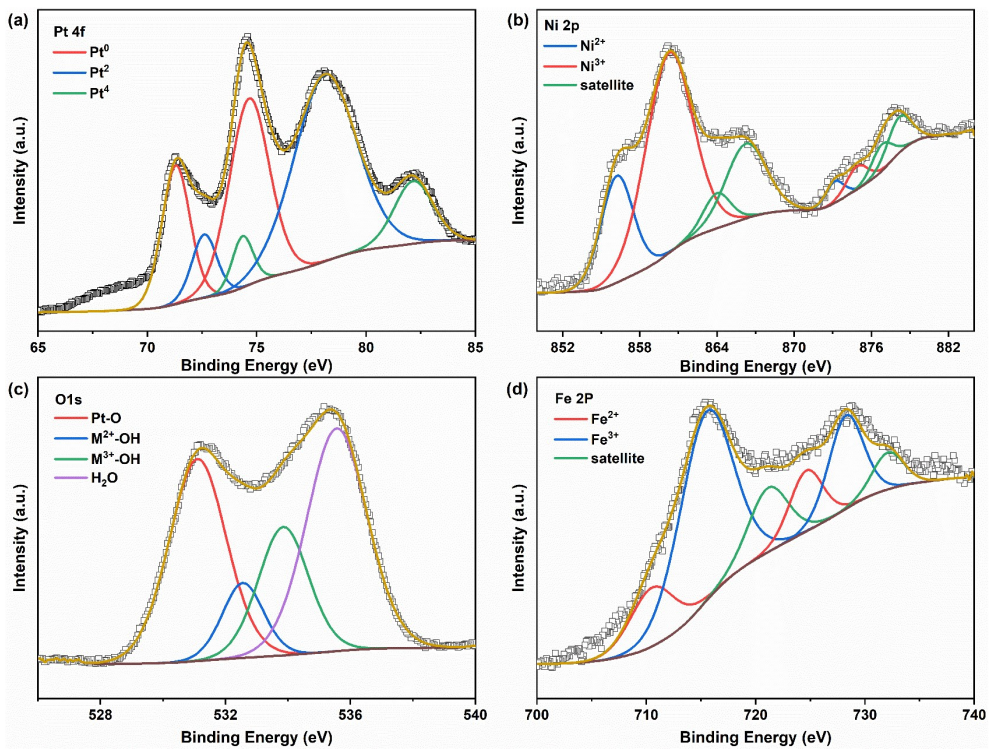


Fig. S13 High-resolution XPS spectra of (a) Pt 4f, (b) Ni 2p, (c)O 1s and (d) Fe 2p for Pt₃Ni₁/NiFe LDHs after OER durability test.

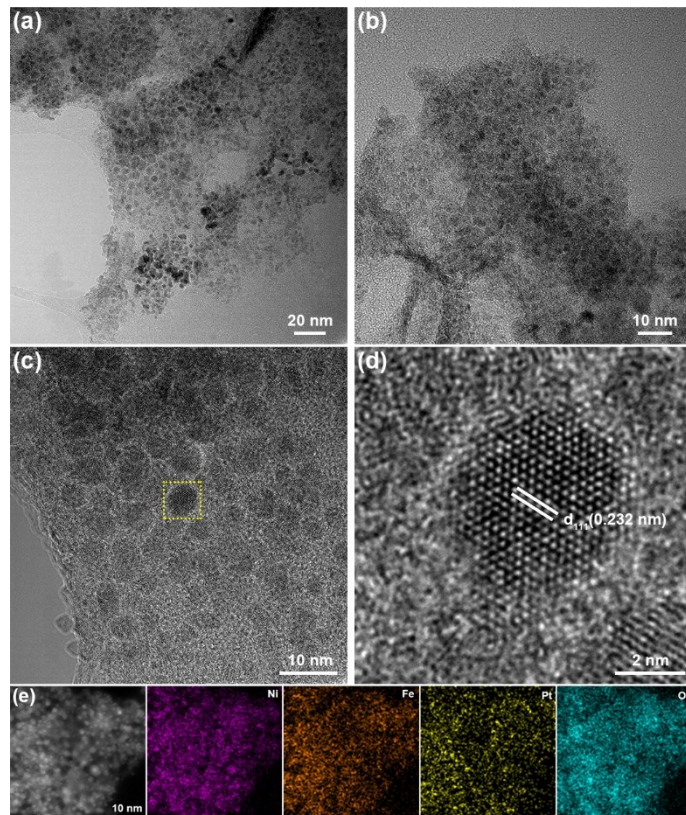


Fig. S14 (a-c) TEM, (d) HRTEM and (e) the corresponding EDS element mapping images of Pt₃Ni₁/NiFe LDHs after OER durability test for 2000 CV cycles.

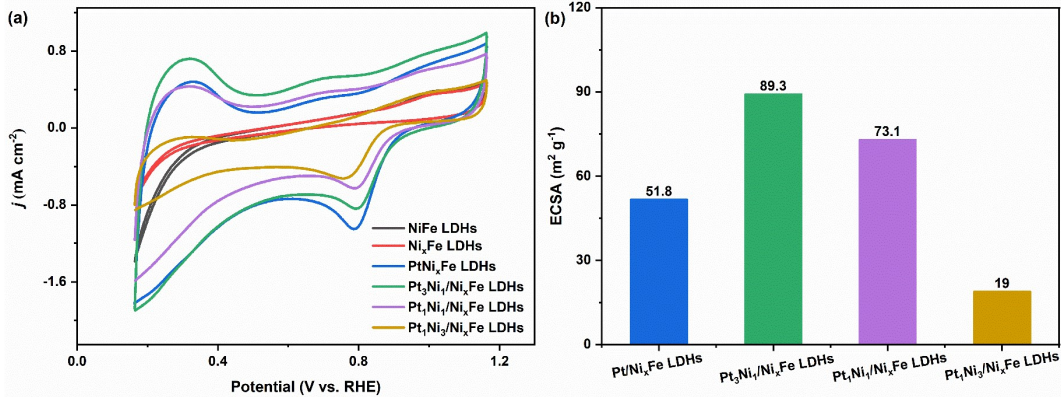


Fig. S15 (a) ORR CV curves of Pt₃Ni₁/Ni_xFe LDHs, Pt₁Ni₁/Ni_xFe LDHs, Pt₁Ni₃/Ni_xFe LDHs, Pt/Ni_xFe LDHs, Ni_xFe LDHs and NiFe LDHs in O₂-saturated 0.1M KOH solutions at a scan rate of 20 mV s⁻¹. (b) Specific ECSAs for Pt₃Ni₁/Ni_xFe LDHs, Pt₁Ni₁/Ni_xFe LDHs, Pt₁Ni₃/Ni_xFe LDHs and Pt/Ni_xFe LDHs.

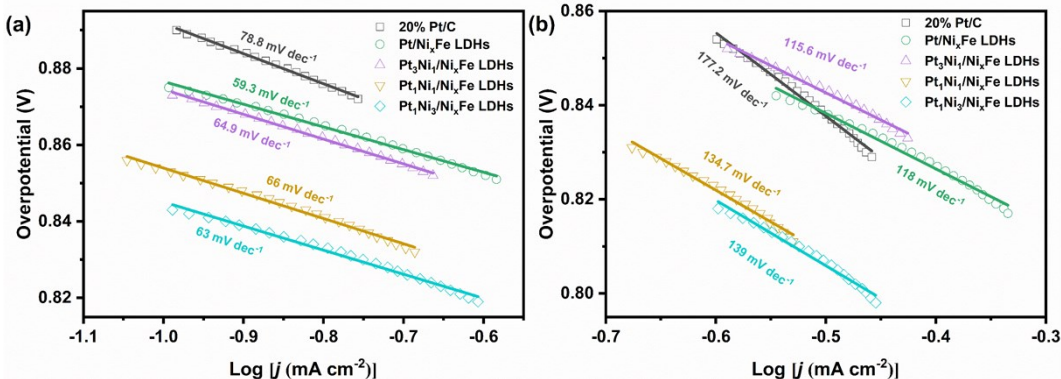


Fig. S16 Tafel plots of Pt₃Ni₁/Ni_xFe LDHs, Pt₁Ni₁/Ni_xFe LDHs, Pt₁Ni₃/Ni_xFe LDHs, Pt/Ni_xFe LDHs and commercial Pt/C catalyst at (a) low overpotential and (b) high overpotential.

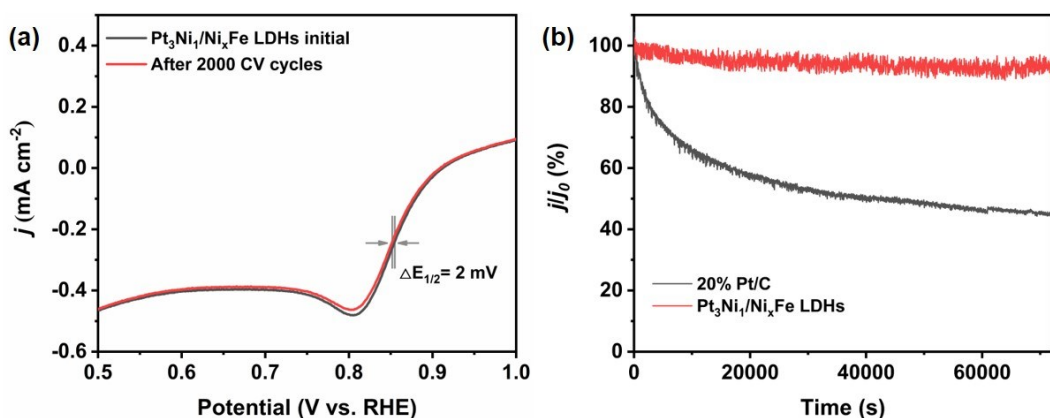


Fig. S17 (a) ORR LSVs of Pt₃Ni₁/Ni_xFe LDHs before and after 2000 CV cycles. (b) ORR stability test at 0.68 V vs. RHE for 20 h.

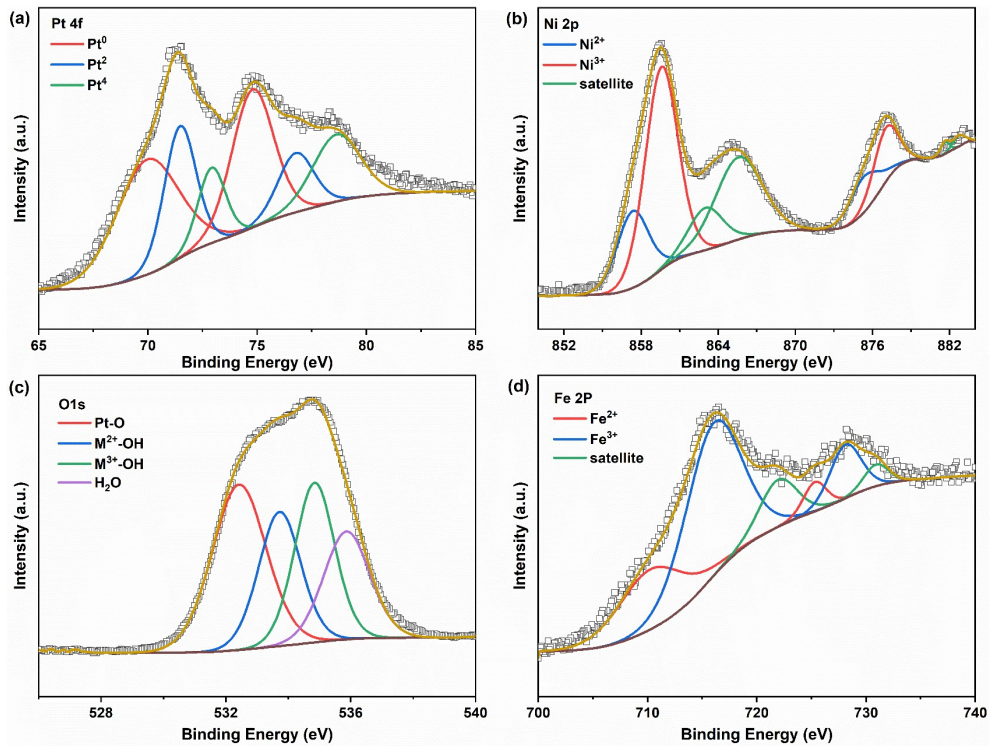


Fig. S18 High-resolution XPS spectra of (a) Pt 4f, (b) Ni 2p, (c) O 1s and (d) Fe 2p for $\text{Pt}_3\text{Ni}_1/\text{NiFe}$ LDHs after ORR durability test.

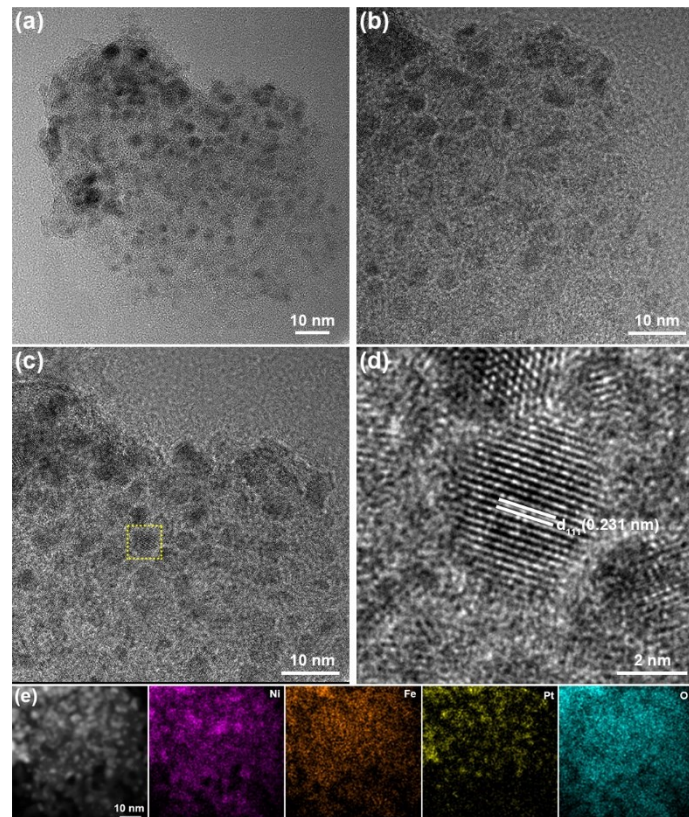


Fig. S19 (a-c) TEM, (d) HRTEM and (e) the corresponding EDS element mapping images of $\text{Pt}_3\text{Ni}_1/\text{NiFe}$ LDHs after ORR durability test for 2000 CV cycles.

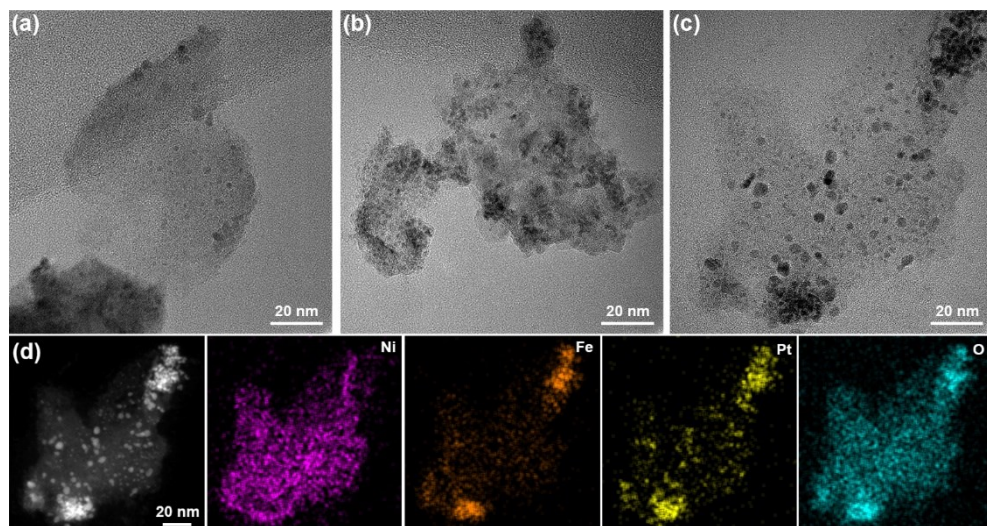


Fig. S20 (a-c) TEM and (d) the corresponding EDS element mapping images of Pt/NiFe LDHs.

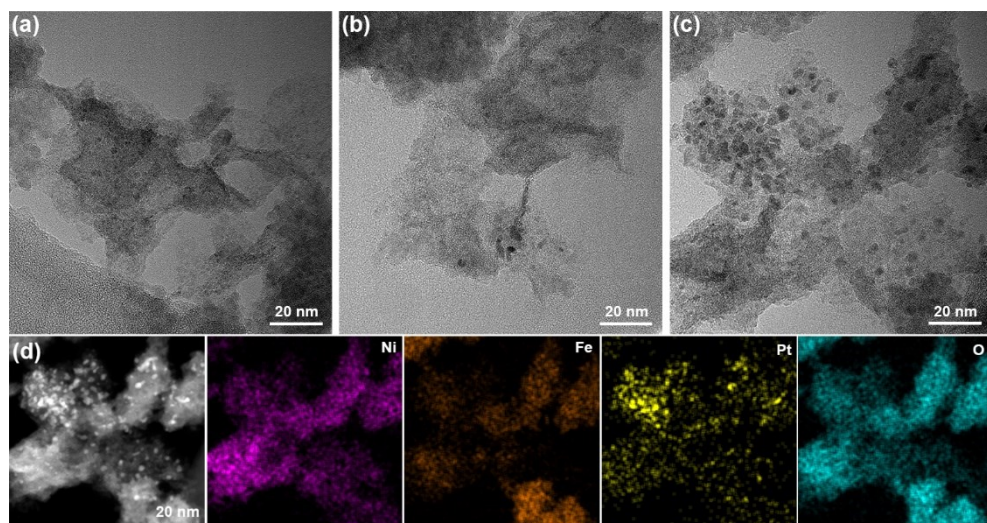


Fig. S21 (a-c) TEM and (d) the corresponding EDS element mapping images of $\text{Pt}_3\text{Ni}_1/\text{NiFe}$ LDHs.

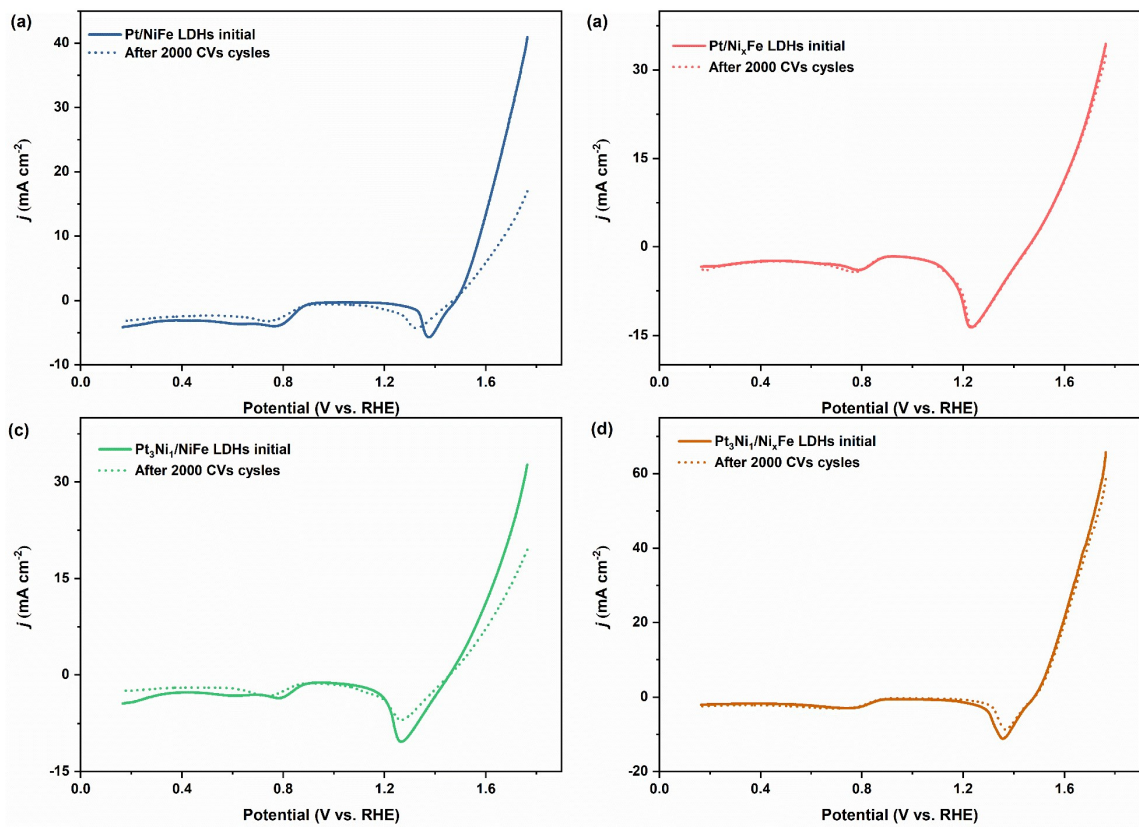


Fig. S22 Polarization curves before and after 2000 CV cycles of (a, b) Pt and (c, d) Pt_3Ni_1 nanoparticles deposited on perfect NiFe LDHs and defects-rich Ni_xFe LDHs.

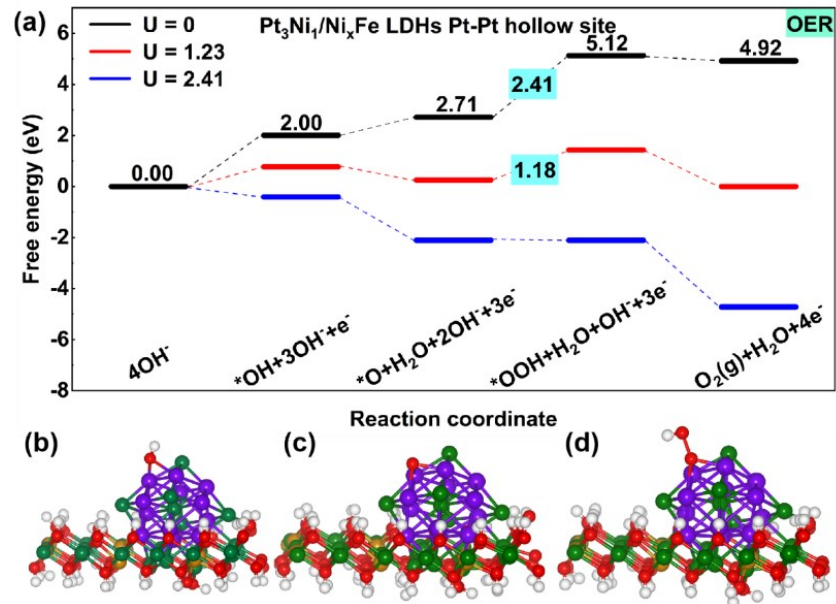


Fig. S23 (a) The free energy profile for the OER pathway of $\text{Pt}_3\text{Ni}_1/\text{Ni}_x\text{Fe}$ LDHs nanosheets. (b) Optimized structures after adsorption of $^*\text{OH}$, $^*\text{O}$ and $^*\text{OOH}$ intermediates on Pt-Pt hollow site of $\text{Pt}_3\text{Ni}_1/\text{Ni}_x\text{Fe}$ LDHs nanosheets. The white, red, brown, green and purple balls represent H, O, Fe, Ni and Pt atoms, respectively.

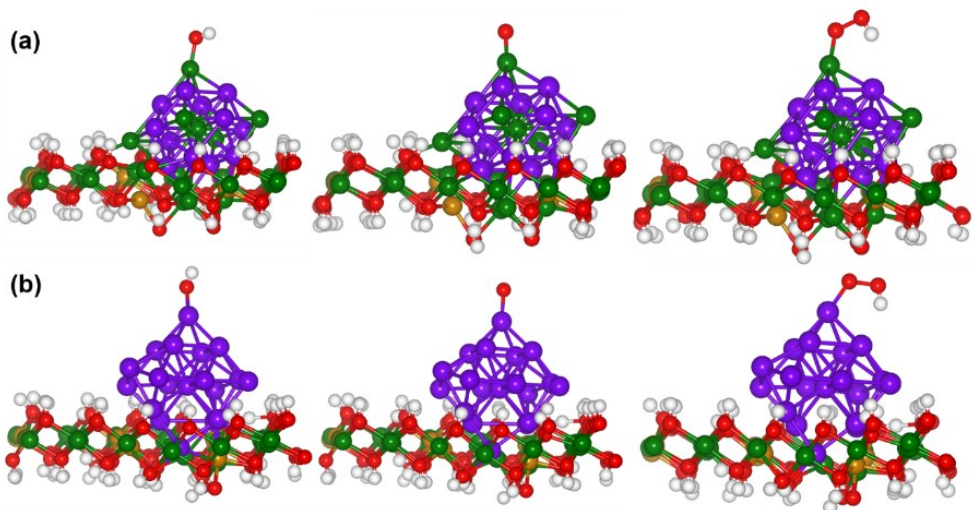


Fig. S24 Optimized structures after adsorption of *OH, *O and *OOH intermediates on (a) Ni top site of $\text{Pt}_3\text{Ni}_1/\text{Ni}_x\text{Fe}$ LDHs nanosheets and (b) Pt top site of $\text{Pt}/\text{Ni}_x\text{Fe}$ LDHs. The white, red, brown, green and purple balls represent H, O, Fe, Ni and Pt atoms, respectively.

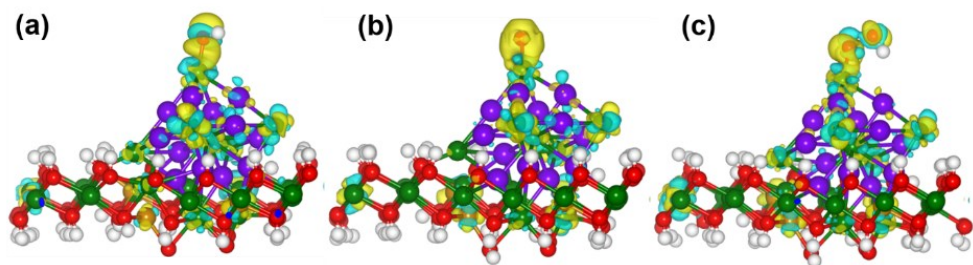


Fig. S25 The charge density difference for *OH (a), *O (b), and *OOH (c) intermediates adsorbed on Ni top site of $\text{Pt}_3\text{Ni}_1/\text{Ni}_x\text{Fe}$ LDHs nanosheets. The white, red, brown, green and purple balls represent H, O, Fe, Ni and Pt atoms, respectively. The yellow (blue) corresponds to charge accumulation (depletion) plotted with an isovalue of $\pm 0.03 \text{ e } \text{\AA}^{-3}$.

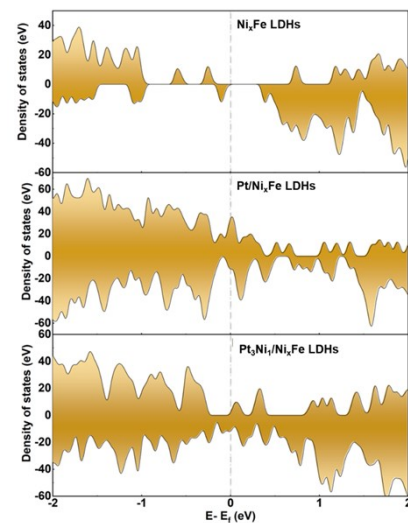


Fig. S26 Calculated density of states (DOS) of defective Ni_xFe LDHs, Pt/ Ni_xFe LDHs and $\text{Pt}_3\text{Ni}_1/\text{Ni}_x\text{Fe}$ LDHs.

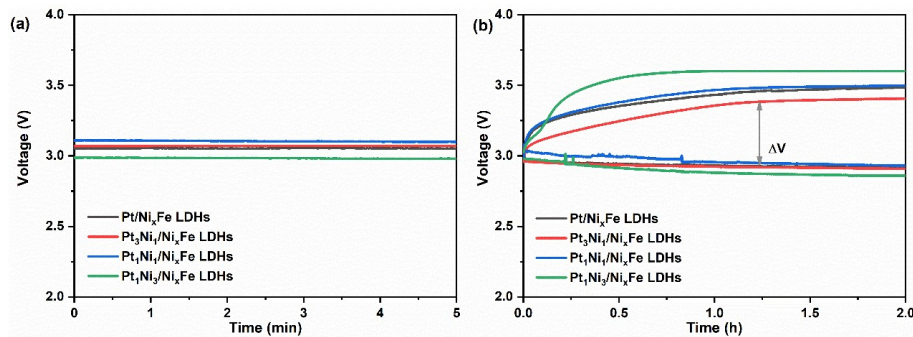


Fig. S27 (a) Open-circuit voltages and (b) charge-discharge curves of HSABs using $\text{Pt}_3\text{Ni}_1/\text{Ni}_x\text{Fe}$ LDHs, $\text{Pt}_1\text{Ni}_1/\text{Ni}_x\text{Fe}$ LDHs, $\text{Pt}_1\text{Ni}_3/\text{Ni}_x\text{Fe}$ LDHs, Pt/ Ni_xFe LDHs as air electrode, respectively.

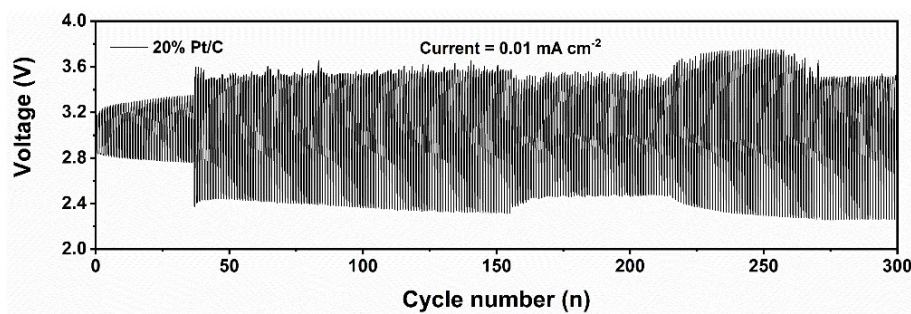


Fig. S28 Cycling stability of hybrid sodium air batteries using 20% Pt/C at a current density of 0.01 mA cm⁻² for 300 cycles.

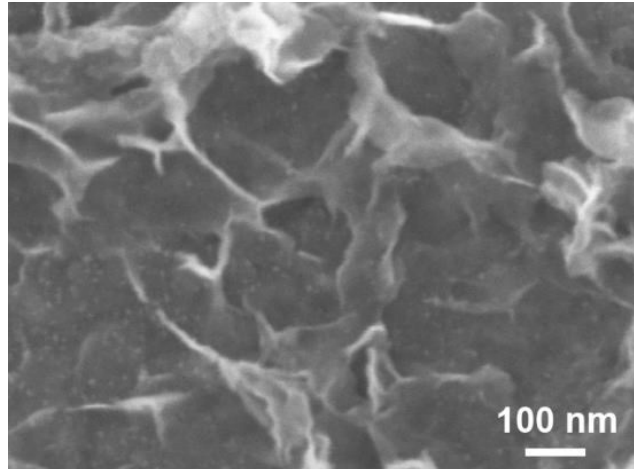


Fig. S29 SEM image of $\text{Pt}_3\text{Ni}_1/\text{Ni}_x\text{Fe}$ LDHs catalysts after long term cycling.

Table S1 Comparison of the bifunctional catalytic activity of as-prepared samples with the recently reported electrocatalysts.

Electrocatalysts	ORR		OER				Reference
	Electrolyte	$E_{1/2}$ (V)	Electrolyte	Tafel slope (mV dec ⁻¹)	η at $j=10$ mA cm ⁻² (V)	η at $j=100$ mA cm ⁻² (V)	
NiFe-LDH/Co _x N-CNF	0.1 M KOH	0.79	0.1 M KOH	60	0.31	-	¹
nNiFe LDH/3D MPC	0.1 M KOH	0.83	0.1 M KOH	71	0.340	-	²
Co ₃ O ₄ @NiFe LDH arrays/Ni foam	-	-	1 M KOH	55.5	-	0.262	³
Single-atom Au/NiFe LDH@Ti mesh	-	-	1 M KOH	36	0.237	-	⁴
Cu@NiFe LDH	-	-	1 M KOH	28	0.199	0.281	⁵
Ag NP/NiRu-LDHs	0.1 M KOH	0.78 (E $j=-3$)	0.1 M KOH	33	0.31	-	⁶
Co ₃ O ₄ -doped Co/CoFe	0.1 M KOH	-	0.1 M KOH	72.8	0.368	-	⁷
Fe-N-C + NiFe-LDH (3:1)	0.1 M KOH	0.79	0.1 M KOH	-	0.31	-	⁸
CoAl-LDH@ZIF-67	0.1 M KOH	0.83	-	-	-	-	⁹
Co SA@NCF/CNF film	0.1 M KOH	0.88	1 M KOH	47	0.4	-	¹⁰
O-NiCoFe-LDH	0.1 M KOH	0.63	0.1 M KOH	93	0.34	-	¹¹
20% Pt/C	0.1 M KOH	0.862	-	-	-	-	This work
20% Ir/C	-	-	1 M KOH	112	0.343	0.547	This work
NiFe LDHs	0.1 M KOH	-	1 M KOH	25.2	0.269	0.479	This work
Ni _x Fe LDHs	0.1 M KOH	-	1 M KOH	21	0.268	0.456	This work
Pt/Ni _x Fe LDHs	0.1 M KOH	0.851	1 M KOH	40.2	0.263	0.442	This work
Pt ₃ Ni ₁ /Ni _x Fe LDHs	0.1 M KOH	0.852	1 M KOH	22	0.265	0.409	This work
Pt ₁ Ni ₁ /Ni _x Fe LDHs	0.1 M KOH	0.84	1 M KOH	27	0.267	0.425	This work
Pt ₁ Ni ₃ /Ni _x Fe LDHs	0.1 M KOH	0.827	1 M KOH	29.1	0.270	0.44	This work

Table S2 Calculated adsorption energy (ΔE_{ads}) for *OH, *O and *OOH intermediates adsorbed on Pt top site of Pt/ Ni_xFe LDHs and Ni top site of $\text{Pt}_3\text{Ni}/\text{Ni}_x\text{Fe}$ LDHs nanosheets.

	E^*_{OH} (eV)	E^*_{O} (eV)	E^*_{OOH} (eV)
Pt/ Ni_xFe LDHs	-0.43	1.05	2.92
$\text{Pt}_3\text{Ni}_1/\text{Ni}_x\text{Fe}$ LDHs	1.09	2.49	3.60

Table S3 Comparison of the hybrid sodium-air batteries performances based on recently reported bifunctional catalysts.

Cathode	Hybrid electrolyte (organic aqueous)	Charge/Discharge voltage (V)	Voltage gap (V)	Roundtrip efficiency (%)	Durability	Reference
MOF-NCNTs	1 M NaClO ₄ in EC/DMC (1:1) with 1 vol% FEC 1 M NaOH	3.10/2.80	0.30	90	35 cycles@0.01 mA cm ⁻²	12
VGC	1 M NaCF ₃ SO ₃ in TEGDME 0.1 M NaOH	3.45/2.81	0.64	81	50 cycles@4 mA g ⁻¹	13
Co ₃ (PO ₄) ₂	1 M NaCF ₃ SO ₃ in TEGDME 0.1 M NaOH	3.41/2.82	0.59	83	50 cycles@0.05 mA cm ⁻²	14
MnO ₂ /rGO/carbon paper	1 M NaCF ₃ SO ₃ in TEGDME 0.1 M NaOH	3.59/2.9	0.7	81	20 cycles@15 mA g ⁻¹	15
S-rGO-CNT-Co	1 M NaCF ₃ SO ₃ in TEGDME Seawater	3.42/3.00	0.42	87.8	50 cycles@0.01 mA cm ⁻²	16
P-Tl ₂ Ru ₂ O ₇	1 M NaCF ₃ SO ₃ in TEGDME 0.1 M NaOH	3.23/3.07	0.16	95	50 cycles@0.01 mA cm ⁻²	17
CuS-CNT	1 M NaClO ₄ in EC/PC with 5% FEC 0.25 M Na ₂ S ₄ /0.1 M NaOH	-	-	90%	100 cycles@0.5 mA cm ⁻²	18
Ni nanoparticles	1 M NaClO ₄ in EC/DMC (1:1) with 1 vol% FEC 1 M NaOH	3.22/2.65	0.57	80.3	100 cycles@0.1 mA cm ⁻²	19
CMO	1 M NaCF ₃ SO ₃ in TEGDME Sea water	3.71/3.13	0.58	84.4	30 cycles@0.01 mA cm ⁻²	20
dp-MnCo ₂ O ₄ /N-rGO	1 M NaClO ₄ in EC/DMC (1:1) with 1 vol% FEC 1 M NaOH	3.14/2.75	0.39	87.6	25 cycles@0.13 mA cm ⁻²	21
SnS ₂	1 M NaCF ₃ SO ₃ in TEGDME 0.1 M NaOH	3.18/2.66	0.52	83%	40 cycles@5 mA g ⁻¹	22
Pt/Ni _x Fe LDHs	1 M NaClO ₄ in TEGDME 0.1 M NaOH	3.48/2.92	0.56	83.9%	-	This work
Pt ₁ Ni ₁ /Ni _x Fe LDHs	1 M NaClO ₄ in TEGDME 0.1 M NaOH	3.50;2.93	0.57	83.7%	-	This work
Pt ₁ Ni ₃ /Ni _x Fe LDHs	1 M NaClO ₄ in TEGDME 0.1 M NaOH	3.60/2.86	0.74	79.4%	-	This work
Pt ₃ Ni ₁ /Ni _x Fe LDHs	1 M NaClO ₄ in TEGDME 0.1 M NaOH	3.41/2.91	0.50	85.4	350 cycles@0.01 mA cm ⁻²	This work

References

1. Q. Wang, L. Shang, R. Shi, X. Zhang, Y. Zhao, G. Waterhouse, L. Wu, C. Tung, T. Zhang, *Adv. Energy Mater.*, 2017, **7**, 1700467.
2. W. Wang, Y. Liu, J. Li, J. Luo, L. Fu, S. Chen, *J. Mater. Chem. A*, 2018, **6**, 14299-14306.
3. X. Guo, X. Hu, D. Wu, C. Jing, W. Liu, Z. Ren, Q. Zhao, X. Jiang, C. Xu, Y. Zhang, N. Hu, *ACS Appl. Mater. Interfaces*, 2019, **11**, 21506-21514.
4. J. Zhang, J. Liu, L. Xi, Y. Yu, N. Chen, S. Sun, W. Wang, K. M. Lange, B. Zhang, *J. Am. Chem. Soc.*, 2018, **140**, 3876-3879.
5. L. Yu, H. Zhou, J. Sun, F. Qin, F. Yu, J. Bao, Y. Yu, S. Chen, Z. Ren, *Energy Environ. Sci.*, 2017, **10**, 1820-1827.
6. S. Chala, M. Tsai, W. Su, K. B. Ibrahim, A. Duma, M. Yeh, C. Wen, C. Yu, T. Chan, H. Dai, B. Hwang, *ACS Cataly.*, 2019, **9**, 117-129.
7. T. Li, Y. Lu, S. Zhao, Z. D. Gao, Y. Song, *J. Mater. Chem. A*, 2018, **6**, 3730-3737.
8. S. Dresp, F. Luo, R. Schmack, S. Kühl, M. Gliech, P. Strasser, *Energy Environ. Sci.*, 2016, **9**, 2020-2024.
9. Z. Li, M. Shao, L. Zhou, R. Zhang, C. Zhang, M. Wei, D. G. Evans, X. Duan, *Adv. Mater.*, 2016, **28**, 2337-2344.
10. D. Ji, L. Fan, L. Li, S. Peng, D. Yu, J. Song, S. Ramakrishna, S. Guo, *Adv. Mater.*, 2019, **31**, 1808267.
11. L. Qian, Z. Lu, T. Xu, X. Wu, Y. Tian, Y. Li, Z. Huo, X. Sun, X. Duan, *Adv. Energy Mater.*, 2015, **5**, 1500245.
12. Y. Wu, X. Qiu, F. Liang, Q. Zhang, A. Koo, Y. Dai, Y. Lei, X. Sun, *Appl. Catal. B Environ.*, 2019, **241**, 407-414.
13. Z. Khan, B. Senthilkumar, S. Park, S. Park, J. Yang, J. Lee, H. Song, Y. Kim, S. Kwak, H. Ko, *J. Mater. Chem. A*, 2017, **5**, 2037-2044.
14. B. Senthilkumar, Z. Khan, S. Park, I. Seo, H. Ko, Y. J. Kim, *J. Power Sources*, 2016, **311**, 29-34.
15. Z. Khan, S. Park, S. M. Hwang, J. Yang, H. Ko, *NPG Asia Mater.*, 2016, **8**, e294.
16. D. Suh, S.. Park, P. Nakhanivej, Y. Kim, S. Hwang, H. Park, *J. Power Sources*, 2017, **372**, 31-37.
17. M. Kim, H. Ju, J. Kim, *Appl. Catal. B Environ.*, 2019, **245**, 29-39.
18. M. Gross, A. Manthiram, *Energy Storage Mater.*, 2019, **19**, 346-351.
19. F. Su, X. Qiu, F. Liang, M. Tanaka, T. Qu, Y. Yao, W. Ma, B. Yang, Y. Dai, K. Hayashi, T. Watanabe, *Nanomaterials*, 2018, **8**, 684.
20. M. Abirami, S.Hwang, J. Yang, S. Senthilkumar, J. Kim, W. Go, B. Senthilkumar, H. Song, Y. Kim, *ACS Appl. Mater. Interfaces*, 2016, **8**, 32778-32787.
21. Y. Kang, D. Zou, J. Zhang, F. Liang, K. Hayashi, H. Wang, D. Xue, K. Chen, K. R. Adair, X. Sun, *Electrochim. Acta*, 2017, **244**, 222-229.
22. Z. Khan, N. Parveen, S. Ansari, S. Senthilkumar, H. Ko, *Electrochim. Acta*, 2017, **257**, 328-334.